NANO LETTERS

pubs.acs.org/NanoLett Letter

All-Sputtered, Superior Power Density Thin-Film Solid Oxide Fuel Cells with a Novel Nanofibrous Ceramic Cathode

Yoon Ho Lee,[▽] Haowen Ren,[▽] Erik A. Wu,[▽] Eric E. Fullerton, Ying Shirley Meng, and Nguyen Q. Minh*

Cite This: https://dx.doi.org/10.1021/acs.nanolett.9b02344 Read Online

ACCESS | Metrics & More | Article Recommendations | Supporting Information

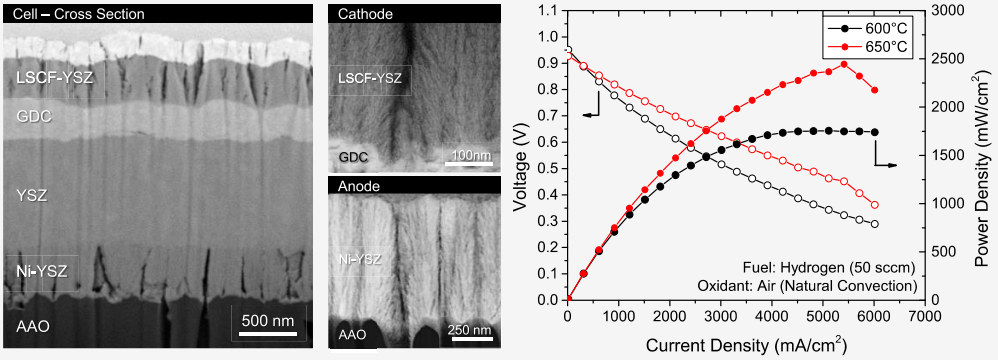

ABSTRACT: Thin film solid oxide fuel cells (TF-SOFCs) are attracting attention due to their ability to operate at comparatively lower temperatures (400−650 °C) that are unattainable for conventional anode-supported SOFCs (650−800 °C). However, limited cathode performance and cell scalability remain persistent issues. Here, we report a new approach of fabricating yttria-stabilized zirconia (YSZ)-based TF-SOFCs via a scalable magnetron sputtering process. Notable is the development and deposition of a porous $La_{0.6}Sr_{0.4}Co_{0.2}Fe_{0.8}O_{2.95}$(LSCF)-based cathode with a unique fibrous nanostructure. This all-sputtered cell shows an open-circuit voltage of ∼1.0 V and peak power densities of ∼1.7 and ∼2.5 W/cm^2 at 600 and 650 °C, respectively, under hydrogen fuel and air along with showing stable performance in short-term testing. The power densities obtained in this work are the highest among YSZ-based SOFCs at these low temperatures, which demonstrate the feasibility of fabricating exceptionally high-performance TF-SOFC cells with distinctive dense or porous nanostructures for each layer, as desired, by a sputtering process. This work illustrates a new, potentially low-cost, and scalable platform for the fabrication of next-generation TF-SOFCs with excellent power output and stability.

KEYWORDS: *Solid oxide fuel cell, SOFC, Thin film, Sputtering, Nanofiber*

INTRODUCTION

Solid oxide fuel cells (SOFCs) have been developed for a broad spectrum of power generation applications.[1] Power systems considered for SOFCs range from watt-sized devices to multimegawatt power plants.[2] Recently, the introduction of nanotechnology has facilitated the development of thin-film SOFCs (TF-SOFCs) and has shown dramatically improved cell performance also allowing for operation for the cell at lower temperatures (e.g., 400−650 °C versus the conventional 650−800 °C).[3] Various deposition processes have been used to fabricate cell components for TF-SOFCs, for example, chemical vapor deposition processes such as atomic layer deposition (ALD) have been shown to be capable of depositing high-quality films.[4−7] However, it is difficult to fabricate porous films required for the anode and cathode using ALD; the structure must be porous for efficient gas supply. To this end, pulsed laser deposition (PLD) has also been used, and ceramic-based TF-SOFCs fabricated via PLD showed high performance and stability.[8,9] However, since it is difficult to use PLD for large area deposition in addition to high maintenance costs, it is preferable to develop a scalable and cost-effective deposition technique such as sputtering for fabricating TF-SOFCs.

Among various physical vapor deposition processes, sputtering is a versatile technique commonly used in mass production as it can create either porous or dense films just by changing the deposition conditions. Several studies have used

Received: June 10, 2019
Revised: January 30, 2020
Published: March 16, 2020

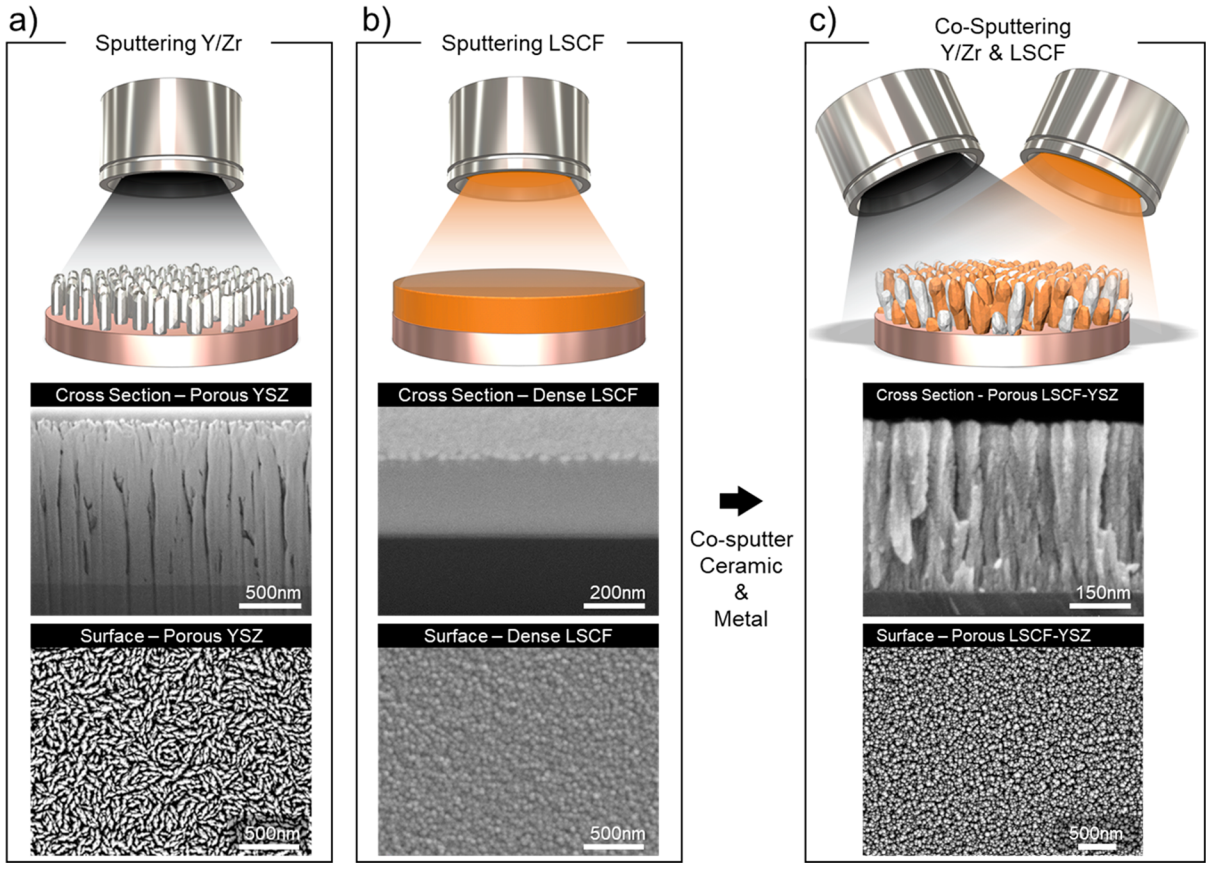

Figure 1. Schematic of sputtering metal, ceramic, and cosputtering of metal and ceramic. (a) Sputtering of a Y/Zr metal alloy target and the corresponding porous YSZ cross-sectional and surface SEM images. (b) Sputtering of a LSCF ceramic target and the corresponding dense LSCF cross-sectional and surface SEM images. (c) Co-sputtering of Y/Zr and LSCF and the corresponding porous LSCF-YSZ cross-sectional and surface SEM images. Two hundred watts was applied to the LSCF ceramic target and 50 W was applied to the Y/Zr target.

sputtering to fabricate TF-SOFCs and showed high performance at relatively low operating temperatures.[10] However, most of these sputtered TF-SOFCs utilized platinum (Pt) as an electrode. Although Pt exhibits high catalytic activity at low temperatures and a porous Pt structure can be made by sputtering,[11] Pt can easily agglomerate at elevated temperatures and thus is not suitable for use at typical SOFC operating temperatures of 650−800 °C.[12] Several approaches have been considered to mitigate this such as cosputtering with ceramics or applying a coating on the Pt surface,[13−15] but the preferable solution is to construct the electrode with a material that is more thermally stable. For this purpose, ceramic-based materials have desirable thermal properties.[16−18] However, it is difficult to make ceramic materials into porous films via sputtering. The most common approach is to sputter using a high pressure of sputtering gas to increase the number of collisions and decrease the kinetic energy of the deposited atoms. This results in low surface mobility of the deposited atoms and the increasing effects of self-shadowing. As the deposition evolves, grains are formed with well-defined and often porous grain boundaries known as zone 1 growth in thin-film deposition.[19] In addition, atoms in the gas can form particle clusters prior to deposition aiding in the formation of porous films. If a porous ceramic electrode can be deposited through sputtering then the entire cell can be fabricated using a single process and a single piece of equipment, which is more cost-effective and beneficial for future mass production of devices.

To illustrate our approach to fabricate a complete SOFC cell by sputtering, yttria-stabilized zirconia (YSZ), Ni-YSZ, and lanthanum strontium cobalt ferrite $La_{0.6}Sr_{0.4}Co_{0.2}Fe_{0.8}O_{2.95}$-YSZ (LSCF-YSZ) are the materials chosen for our electrolyte, anode, and cathode, respectively, as they are materials which have been shown to have good performance in SOFC applications. Apart from that, a high activation energy owing to the oxygen reduction reaction (ORR) at the interface of cathode and electrolyte is a persistent problem in most SOFC devices. To reduce the activation energy of ORR, using a gadolinia-doped ceria (GDC) cathode functional interlayer sandwiched between the cathode and electrolyte (that can be fabricated by magnetron sputtering[20,21]) is one of the simplest approaches that can be applied in our process.

For TF-SOFCs, the substrate plays a very important role. If the substrate pore size is small and uniform, a thin cell without cracks and defects can be produced on the substrate with sufficient fuel mass transport. From this point of view, anodized aluminum oxide (AAO) substrates are a suitable support upon which thin films, especially thin-film electrolytes, can be deposited.[22,23] AAO is made by anodizing an aluminum sheet where pores of several tens of nanometers are formed and uniformly distributed. Depending on the anodic oxidation conditions, the size of the pore and thus the porosity of the film can be easily manipulated. The tortuosity of AAO can be very low due to the straight and aligned pore structure through the substrate. This ultimately enables fuel to be sufficiently

https://dx.doi.org/10.1021/acs.nanolett.9b02344
Nano Lett. XXXX, XXX, XXX−XXX

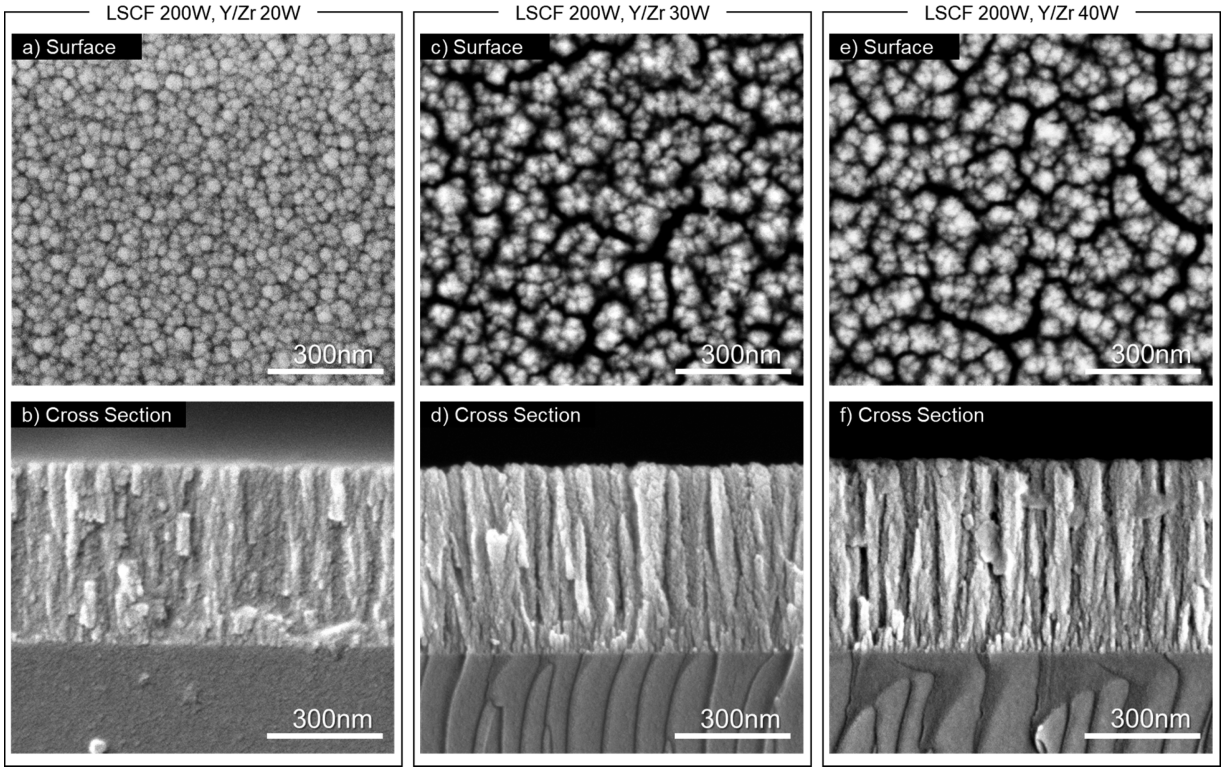

Figure 2. Surface and cross-sectional images of LSCF-YSZ with different LSCF-to-YSZ ratios. (a) Surface and (b) cross sectional FE-SEM image of LSCF-YSZ deposited by cosputtering at 200 W for LSCF and 20 W for Y/Zr. (c) Surface and (d) cross sectional FE-SEM image of LSCF-YSZ deposited at 200 W for LSCF and 30 W for Y/Zr. (e) Surface and (f) cross sectional FE-SEM image of LSCF-YSZ deposited at 200 W for LSCF and 40 W for Y/Zr.

supplied to the cell even with a pore size as small as several tens of nanometers.

In this work, we describe a new method of the development of a porous ceramic nanostructure for SOFC electrodes and incorporate it into a full cell by sputtering at room temperature in a single sputtering process. Characterization of the cells shows fully dense layers for the electrolyte and cathode functional interlayer and well-defined and distinctive nanostructures for the electrodes. These cells exhibit exceptional power densities, to the best of our knowledge, the highest recorded performance for a YSZ-based SOFC, and this sputtering method can be applied to all kinds of different combinations of materials for porous electrodes, especially the cathode, in TF-SOFCs.

RESULTS

Development of the Porous LSCF-YSZ Cathode. Depositing LSCF via ceramic sputtering targets usually results in a dense structure owing to a rare atomic shadowing effect.[19] In this case, directly sputtering ceramic LSCF electrode can only result in dense films as shown in Figure 1b, no matter if the sputtering process parameters were changed. Alternatively, a metallic yttrium/zirconium (Y/Zr) alloy film through direct current (DC) sputtering can easily yield columnar growth of the Y/Zr alloy, which in turn has a much lower adatom mobility, thus a better atomic shadowing effect. Ultimately, this effect results in a porous structure (Figure 1a). Taking inspiration from this result, it follows that it could be possible to sputter two materials together, or cosputter, to fabricate a porous LSCF-YSZ cathode. Co-sputtering was previously used to create composite films such as Ni-YSZ anode composites.[24] Thus, cosputtering of LSCF and Y/Zr could also be used to create a porous cathode structure.

To fabricate a porous LSCF-based electrode, cosputtering of Y/Zr metal alloy and LSCF targets was performed. Since Y/Zr can be easily formed into a porous film at high Ar pressures, the cosputtering of LSCF and Y/Zr could yield a porous film of LSCF-YSZ using similar conditions. The resulting cosputtered LSCF-YSZ film has a porous, columnar nanostructure as shown in the SEM images in Figure 1c. According to the images, this columnar structure has a diameter of tens of nanometers, thus creating a very large active surface area.

The desired growth mechanism takes place as long as the following occur at the start of cosputtering: (1) Atoms sputtered from Y/Zr target combine into a cluster of particles at high pressure in the chamber. This leads to a low adatom mobility in sputtered Y/Zr atoms and they are more likely to create many well-separated growing nuclei on the room temperature substrate. (2) LSCF with a lower volume ratio prefers to stay on the surface of the Y/Zr (this is aided further by oxygen atoms).[25] (3) A high-processing Ar pressure scatters the sputtered atoms in the chamber, making atoms sputter at larger angles. This enhances the sputtering rate at high points but lowers the rate at valleys due to the shadowing effect, which in turn makes columnar growth more dominant.

To fully understand the growth mechanism of the porous columnar LSCF-YSZ shown in Figure 1c, LSCF-YSZ was deposited with different LSCF-to-Y/Zr ratios (Figure 2). The power applied to the LSCF target was fixed to 200 W and the power applied to the Y/Zr target was varied to compare the microstructure of various LSCF-YSZ cosputtered composites.

https://dx.doi.org/10.1021/acs.nanolett.9b02344
Nano Lett. XXXX, XXX, XXX−XXX

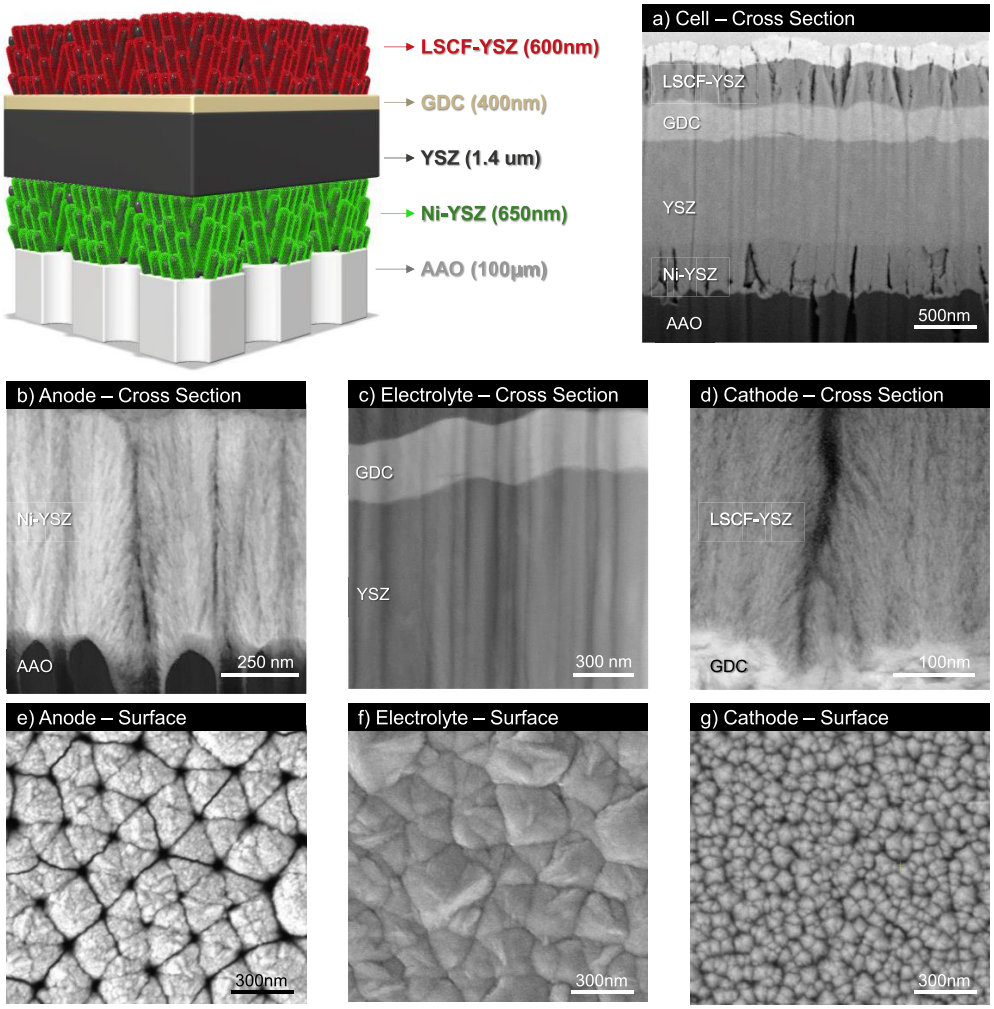

Figure 3. Schematic of the cell architecture. (a) Cross section FE-SEM image of the cell architecture. STEM view of the (b) anode, (c) electrolyte with interlayer, and (d) cathode, respectively. Respective FE-SEM surface images of (e) Ni-YSZ layer on AAO, (f) GDC layer on top of AAO/Ni-YSZ/YSZ, and (g) LSCF-YSZ layer on top of AAO/Ni-YSZ/YSZ/GDC.

According to the images of LSCF-YSZ deposited at 20 W for Y/Zr (Figure 2a,b), a mesoporous structure was seen on the surface image, but the cross-sectional image showed that the pores were not fully connected through the cathode to the interface of the substrate. Thus, although such an electrode would have a large surface area, without continuous pores, air could not be efficiently delivered to the triple phase boundary (TPB). When the Y/Zr target is increased to 30 W, the size of the particles increased by about two times and the microstructure became relatively more porous. However, discontinuous pores are also similarly observed for the 30 W-sputtered Y/Zr. While the surface image of LSCF-YSZ deposited with 40 W Y/Zr power was similar to that of the film deposited at 30 W, the nanostructure observed by the cross-sectional image for 40 W Y/Zr was different; at 40 W, the pores have become completely continuous from the inlet to the substrate surface. As the number of particles of metallic Y/Zr increased during the deposition of LSCF-YSZ, the higher rate of the shadowing effect resulted in a columnar structure with greater porosity.

Through calculating the LSCF and YSZ deposition rates, it was confirmed that if the YSZ content of LSCF-YSZ exceeds about 50%, the thin film will show a highly porous columnar structure. Our LSCF-YSZ used for cell fabrication was deposited at 50 W for Y/Zr and 200 W for LSCF. This increase to 50 W, which meant that the YSZ content is slightly higher than that at the 40 W critical point, was chosen so that a porous film can be fabricated consistently and reliably. Figure 1c illustrates the morphology using these conditions.

According to the XRD analysis as shown in Figure S1, peaks from LSCF and YSZ are observed and the nonconducting secondary phases of $La_2Zr_2O_7$ and $SrZrO_3$ were not generated. This is due to the room-temperature deposition and 600 °C annealing; the thermal energy of the plasma during sputtering was not sufficient to support the formation of secondary phases.[21]

Full Cell Fabrication and Characterization. The anode, electrolyte, interlayer, and cathode were sequentially sputtered onto the porous AAO and shown schematically in Figure 3 and the corresponding STEM micrograph in Figure 3a. Figure 3b–d shows the STEM images and Figure 3e–g shows the corresponding SEM images of the surface morphology of each component. With this configuration, no etching or patterning steps were required between sputtering of the different films. One clear benefit was that the samples were kept under vacuum during the fabrication process, especially for complete cells, and thus ambient contamination was minimized since sputtering was done sequentially in the same chamber.

https://dx.doi.org/10.1021/acs.nanolett.9b02344
Nano Lett. XXXX, XXX, XXX−XXX

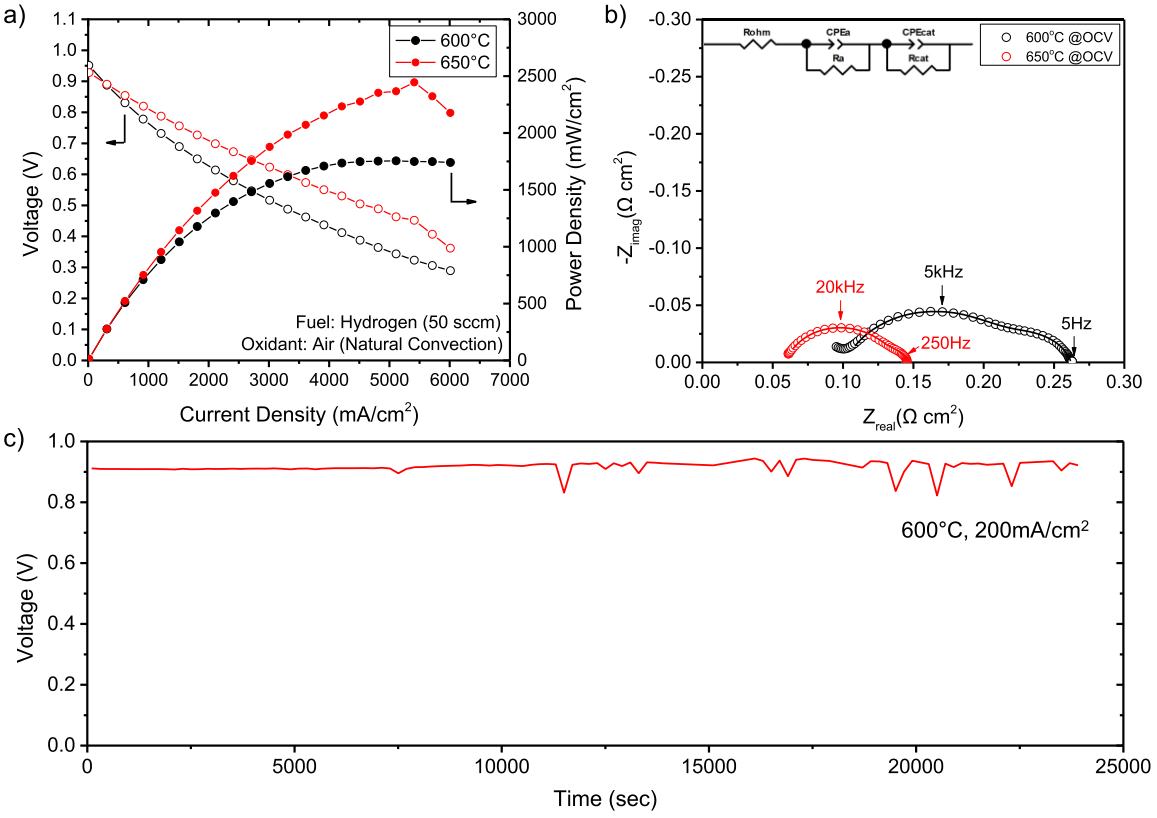

Figure 4. (a) Current−voltage (I−V) and current−power (I−P) curves and (b) EIS measurement of the TF-SOFC with hydrogen fuel and air at 600 and 650 °C, respectively. The lines on the Nyquist plot correspond to the respective fits from the equivalent circuit in the inset. (c) Short-term stability test; the cell voltage was measured over time while applying a constant current of 200 mA/cm^2.

A 700 nm Ni-YSZ porous anode layer was deposited onto the AAO. As shown in Figure 3a,b, the Ni-YSZ electrode is formed as a collection of larger columns with a diameter of about 200 nm with smaller columns of less than 10 nm in diameter on top of the 200 nm columns. The surface morphology of Ni-YSZ (Figure 3e) showing hexagonally arranged columns that do not completely block the pores of the AAO. This microstructure provides a very high active surface area for the anode, thus significantly improving electrode performance. Figure S2a shows the distribution of the elements through STEM-EDX analysis of the Ni-YSZ electrode. The YSZ electrolyte and the GDC interlayer were deposited on top of the Ni−YSZ anode. As seen in Figure 3a, the YSZ electrolyte has a thickness of about 1.4 μm, relatively thick considering a previous report of 150 nm YSZ electrolytes applied to AAO-based SOFCs.[7] While thin electrolytes can increase performance, the trade-off is that structural defects in fabrication leading to cell failure during operation is more likely to occur. Since structural defects occur in proportion to the cell area, this issue is significantly exacerbated when applying an ultrathin electrolyte to a large-active-area cell. With these considerations, a relatively thick electrolyte was applied in this study. Even with a high electrolyte thickness, the cells are still capable of achieving exceptional power densities.

A GDC interlayer[26] was deposited between the electrolyte and the cathode. Both the sputtering power and substrate location in the chamber were varied for GDC. The properties of the GDC interlayer are shown in Figures S3−S6. By tuning the power and substrate location in the chamber, dense, and uniform GDC layers resulted. Such a GDC interlayer was applied to the cells as illustrated in Figure 3a−c.

The LSCF-YSZ cathode was then deposited on the top of the GDC interlayer (Figure 3d−g). The LSCF-YSZ shows an extremely fine nanofibrous structure with a diameter of less than 10 nm and relatively large openings between the columns, which ensures high mass transport of oxygen to the whole cathode as well as a large active surface area. As the LSCF target has a composition of $La_{0.6}Sr_{0.4}Co_{0.2}Fe_{0.8}O_{2.95}$, STEM-EDX of LSCF-YSZ in Figure S2b shows that the signals from La and Fe are more intense than those of Sr and Co; however, to examine the exact stoichiometry of the sputtered LSCF films, further work involving different characterization techniques is required. The SEM, STEM, and STEM-EDX results nevertheless show that each component of the TF-SOFC with distinct nanostructures have been successfully deposited via magnetron sputtering.

Cell Performance. Electrochemical analysis of the TF-SOFC is shown in Figure 4 and a schematic of the test cell setup is shown in Figure S7. The cell has active area of 1 mm^2 (1 mm × 1 mm) and was tested under pure hydrogen at a flow rate of 50 sccm and exposed to air for the oxygen source. Our tested cells show an open-circuit voltage (OCV) of ∼0.95 V and a peak power density of ∼1.7 and ∼2.5 W/cm^2 at 600 and 650 °C, respectively (Figure 4a), the highest recorded power density for YSZ-based SOFC devices. According to the EIS measurement shown in Figure 4b, relatively low polarization losses were observed at both 600 and 650 °C. Since the cosputtered Ni-YSZ electrode and the LSCF-YSZ electrodes consist of nanofibers of less than 10 nm in diameter, the number of reaction sites in the electrodes were significantly increased. In conjunction with Figure 3a,b,d, since the relatively larger vertical pores are formed in the electrodes at

https://dx.doi.org/10.1021/acs.nanolett.9b02344
Nano Lett. XXXX, XXX, XXX−XXX

every 100−200 nm, the fine microstructure among these larger pores ultimately results in more effective gas delivery.

In terms of materials, a mixture of LSCF and YSZ will increase the triple phase boundary compared to pure LSCF electrodes. Since YSZ has low electrical conductivity, it is required to analyze the effect of the YSZ mixture in LSCF in terms of electrical conductivity and polarization losses. According to the comparison in Figure S8, the peak power density for the TF-SOFC with pure LSCF as the cathode was about 550 mW/cm^2 at 600 °C, about a third of that compared to the LSCF-YSZ composite at the same temperature. According to the EIS fitting results in Table S1, although pure LSCF has a lower ohmic resistance by about 0.05 Ω cm^2, its overall polarization resistance (R_{cat+} R_{pol}) is much greater (by over 1 Ω cm^2). In other words, even though cosputtering of YSZ with LSCF slightly increases the ohmic resistance, it drastically reduces the polarization loss, which is consistent with the increased cell performance and peak power density measurements.

In order to investigate the cell durability or the cell performance over time, the voltage was measured at a constant current of 200 mA/cm^2 at 600 °C and the results are shown in Figure 4c. This short-term stability test was performed for about 7 h where the cell showed a constant voltage without significant degradation. It should be noted that if the cell was operated at the peak power density for extended periods of time without air cooling, the cells tended to fail because of the large amount of heat generated from the high current density.

Lastly, it is important to note that previously AAO-based TF-SOFCs used Pt electrodes; thus the operating temperature was restricted to 400−500 °C to avoid Pt nanoparticle agglomeration.[3−7,10,12−14,22−24,27−29] In this study, by using Ni-YSZ and LSCF-YSZ as the anode and cathode respectively, the cells were able to be tested at 600−650 °C without significant performance degradation. A comparison of our cell performance with other reports on AAO-based TF-SOFCs, power densities for anode-supported YSZ-based cells, as well as other cell configurations can be found in Figures S9−S11.

SUMMARY

In summary, TF-SOFCs (~3 μm thick) on AAO substrates were fabricated via a sputtering process for all of the cell components, which were composed of conventional materials (YSZ for the electrolyte, GDC for the electrolyte/cathode interlayer, Ni-YSZ for the anode, and LSCF-YSZ for the cathode). Fully dense YSZ and GDC films, along with porous Ni-YSZ and LSCF-YSZ films with columnar nanostructures (that yield a high active surface area) were successfully developed and fabricated. Electrochemical evaluations of the cell showed an OCV of ~1.0 V and exceptional peak power densities of ~1.7 and ~2.5 W/cm^2 with hydrogen fuel and air at 600 and 650 °C, respectively. Further work is ongoing to refine the cell architecture, optimize and scale up the fabrication process, evaluate long-term performance stability, and investigate cell operation with different hydrocarbon fuels.

ASSOCIATED CONTENT

Supporting Information

The Supporting Information is available free of charge at https://pubs.acs.org/doi/10.1021/acs.nanolett.9b02344.

Detailed experimental procedures (PDF)

AUTHOR INFORMATION

Corresponding Author

Nguyen Q. Minh − *Center for Energy Research, University of California, San Diego, La Jolla, California 92093, United States;* orcid.org/0000-0003-3276-6150; Email: nminh@ucsd.edu

Authors

Yoon Ho Lee − *Center for Energy Research, University of California, San Diego, La Jolla, California 92093, United States;* orcid.org/0000-0003-1795-7872

Haowen Ren − *Materials Science and Engineering, University of California, San Diego, La Jolla, California 92093, United States*

Erik A. Wu − *Department of Nanoengineering, University of California, San Diego, La Jolla, California 92093, United States*

Eric E. Fullerton − *Materials Science and Engineering, Department of Nanoengineering, Center for Memory and Recording Research, Sustainable Power and Energy Center (SPEC), and Department of Electrical and Computer Engineering, University of California, San Diego, La Jolla, California 92093, United States*

Ying Shirley Meng − *Department of Nanoengineering, Center for Memory and Recording Research, and Sustainable Power and Energy Center (SPEC), University of California, San Diego, La Jolla, California 92093, United States;* orcid.org/0000-0001-8936-8845

Complete contact information is available at: https://pubs.acs.org/10.1021/acs.nanolett.9b02344

Author Contributions

[▽]Y.H.L., H.R., and E.A.W. equally contributed to this work.

Notes

The authors declare no competing financial interest.

ACKNOWLEDGMENTS

This work is funded by the U.S. Department of Energy/National Energy Technology Laboratory (DOE/NETL) under the Cooperative Agreement DE-FE0026211. This work was performed in part at the San Diego Nanotechnology Infrastructure (SDNI) of University of California, San Diego (UCSD), a member of the National Nanotechnology Coordinated Infrastructure, which is supported by the National Science Foundation under Grant ECCS-1542148. STEM and STEM-EDX were performed at the University of California, Irvine Materials Research Institute (IMRI) using instrumentation funded in part by the National Science Foundation Major Research Instrumentation Program under Grant CHE-1338173. We would like to thank Ms. Hyeseung Chung of the UCSD Department of Nanoengineering for aiding with the collection of the STEM and STEM-EDX data.

REFERENCES

(1) Minh, N. Q. Cell and stack design, fabrication and performance. In *High-Temperature Solid Oxide Fuel Cells for the 21st Century*; Kendall, K., Kendall, M., Eds.; Academic Press: London, 2015.

(2) Minh, N. Q. System designs and applications. In *High-Temperature Solid Oxide Fuel Cells for the 21st Century*; Kendall, K., Kendall, M., Eds.; Academic Press: London, 2015.

(3) Evans, A.; Bieberle-Hütter, A.; Rupp, J. L. M.; Gauckler, L. J. Review on Microfabricated Micro-Solid Oxide Fuel Cell Membranes. *J. Power Sources* **2009**, *194* (1), 119−129.

(4) Shim, J. H.; Park, J. S.; An, J.; Gür, T. M.; Kang, S.; Prinz, F. B. Intermediate-Temperature Ceramic Fuel Cells with Thin Film

Yttrium-Doped Barium Zirconate Electrolytes. *Chem. Mater.* **2009**, *21* (14), 3290−3296.
(5) Su, P.-C.; Chao, C.-C.; Shim, J. H.; Fasching, R.; Prinz, F. B. Solid Oxide Fuel Cell with Corrugated Thin Film Electrolyte. *Nano Lett.* **2008**, *8* (8), 2289−2292.
(6) An, J.; Kim, Y. B.; Park, J.; Gür, T. M.; Prinz, F. B. Three-Dimensional Nanostructured Bilayer Solid Oxide Fuel Cell with 1.3 W/cm^2 at 450°C. *Nano Lett.* **2013**, *13* (9), 4551−4555.
(7) Ji, S.; Cho, G. Y.; Yu, W.; Su, P.-C.; Lee, M. H.; Cha, S. W. Plasma-Enhanced Atomic Layer Deposition of Nanoscale Yttria-Stabilized Zirconia Electrolyte for Solid Oxide Fuel Cells with Porous Substrate. *ACS Appl. Mater. Interfaces* **2015**, *7* (5), 2998−3002.
(8) Ju, Y.-W.; Jun, A.; Inoishi, A.; Ida, S.; Lim, T.; Kim, G.; Ishihara, T. Growth of Thin-Film Layered Perovskite Cathodes by Pulsed Laser Deposition and Their Electrochemical Studies in IT-SOFCs. *J. Electrochem. Soc.* **2014**, *161* (6), F698−F702.
(9) Wang, F.; Brito, M. E.; Yamaji, K.; Cho, D. H.; Nishi, M.; Kishimoto, H.; Horita, T.; Yokokawa, H. Effect of Polarization on Sr and Zr Diffusion Behavior in LSCF/GDC/YSZ System. *Solid State Ionics* **2014**, *262*, 454−459.
(10) Tsuchiya, M.; Lai, B. K.; Ramanathan, S. Scalable Nanostructured Membranes for Solid-Oxide Fuel Cells. *Nat. Nanotechnol.* **2011**, *6* (5), 282−286.
(11) Chang, I.; Woo, S.; Lee, M. H.; Shim, J. H.; Piao, Y.; Cha, S. W. Characterization of Porous Pt Films Deposited via Sputtering. *Appl. Surf. Sci.* **2013**, *282*, 463−466.
(12) Wang, X.; Huang, H.; Holme, T.; Tian, X.; Prinz, F. B. Thermal Stabilities of Nanoporous Metallic Electrodes at Elevated Temperatures. *J. Power Sources* **2008**, *175* (1), 75−81.
(13) Chang, I.; Ji, S.; Park, J.; Lee, M. H.; Cha, S. W. Ultrathin YSZ Coating on Pt Cathode for High Thermal Stability and Enhanced Oxygen Reduction Reaction Activity. *Adv. Energy Mater.* **2015**, *5* (10), 1402251.
(14) Lee, Y. H.; Cho, G. Y.; Chang, I.; Ji, S.; Kim, Y. B.; Cha, S. W. Platinum-Based Nanocomposite Electrodes for Low-Temperature Solid Oxide Fuel Cells with Extended Lifetime. *J. Power Sources* **2016**, *307*, 289−296.
(15) Choi, H. J.; Kim, M.; Neoh, K. C.; Jang, D. Y.; Kim, H. J.; Shin, J. M.; Kim, G. T.; Shim, J. H. High-Performance Silver Cathode Surface Treated with Scandia-Stabilized Zirconia Nanoparticles for Intermediate Temperature Solid Oxide Fuel Cells. *Adv. Energy Mater.* **2017**, *7* (4), 1601956.
(16) Minh, N. Q. Ceramic Fuel Cells. *J. Am. Ceram. Soc.* **1993**, *76* (3), 563−588.
(17) O'Hayre, R.; Cha, S.-W.; Colella, W.; Prinz, F. B. *Fuel Cell Fundamentals*; John Wiley & Sons: New York, 2006.
(18) Noh, H.-S.; Son, J.-W.; Lee, H.; Ji, H.-I.; Lee, J.-H.; Lee, H.-W. Suppression of Ni Agglomeration in PLD Fabricated Ni-YSZ Composite for Surface Modification of SOFC Anode. *J. Eur. Ceram. Soc.* **2010**, *30* (16), 3415−3423.
(19) Thornton, J. A. The Microstructure of Sputter□deposited Coatings. *J. Vac. Sci. Technol., A* **1986**, *4* (6), 3059−3065.
(20) Gong, Y.; Ji, W.; Zhang, L.; Li, M.; Xie, B.; Wang, H.; Jiang, Y.; Song, Y. Low Temperature Deposited (Ce, Gd)O_{2-x} Interlayer for $La_{0.6}$ $Sr_{0.4}$ $Co_{0.2}$ $Fe_{0.8}$ O_3 Cathode Based Solid Oxide Fuel Cell. *J. Power Sources* **2011**, *196* (5), 2768−2772.
(21) Jung, W.; Kim, J. J.; Tuller, H. L. Investigation of Nanoporous Platinum Thin Films Fabricated by Reactive Sputtering: Application as Micro-SOFC Electrode. *J. Power Sources* **2015**, *275*, 860−865.
(22) Kwon, C.-W.; Son, J.-W.; Lee, J.-H.; Kim, H.-M.; Lee, H.-W.; Kim, K.-B. High-Performance Micro-Solid Oxide Fuel Cells Fabricated on Nanoporous Anodic Aluminum Oxide Templates. *Adv. Funct. Mater.* **2011**, *21* (6), 1154−1159.
(23) Park, J.; Lee, Y.; Chang, I.; Lee, W.; Cha, S. W. Engineering of the Electrode Structure of Thin Film Solid Oxide Fuel Cells. *Thin Solid Films* **2015**, *584*, 125−129.
(24) Cho, G. Y.; Lee, Y. H.; Cha, S. W. Multi-Component Nano-Composite Electrode for SOFCS via Thin Film Technique. *Renewable Energy* **2014**, *65*, 130−136.
(25) Leamy, H. J.; Dirks, A. G. Microstructure and Magnetism in Amorphous Rare-Earth−Transition-Metal Thin Films. I. Microstructure. *J. Appl. Phys.* **1978**, *49* (6), 3430−3438.
(26) Kim, W.-H.; Song, H.-S.; Moon, J.; Lee, H.-W. Intermediate Temperature Solid Oxide Fuel Cell Using (La, Sr)(Co, Fe)O_3-Based Cathodes. *Solid State Ionics* **2006**, *177* (35−36), 3211−3216.
(27) Hong, S.; Bae, J.; Koo, B.; Kim, Y. B. High-Performance Ultra-Thin Film Solid Oxide Fuel Cell Using Anodized-Aluminum-Oxide Supporting Structure. *Electrochem. Commun.* **2014**, *47*, 1−4.
(28) Lim, Y.; Hong, S.; Bae, J.; Yang, H.; Kim, Y. B. Influence of Deposition Temperature on the Microstructure of Thin-Film Electrolyte for SOFCs with a Nanoporous AAO Support Structure. *Int. J. Hydrogen Energy* **2017**, *42* (15), 10199−10207.
(29) Lee, Y. H.; Chang, I.; Cho, G. Y.; Park, J.; Yu, W.; Tanveer, W. H.; Cha, S. W. Thin Film Solid Oxide Fuel Cells Operating Below 600°C: A Review. *International J. Precis. Eng. Manuf. Technol.* **2018**, *5* (3), 441−453.

https://dx.doi.org/10.1021/acs.nanolett.9b02344
Nano Lett. XXXX, XXX, XXX−XXX